EXTRACTION ABILITY OF LANTHANIDE RARE EARTH IONS BY AZACROWN ETHER IN SULFATE SOLUTION

Jianghua WU[1,2], Duchao ZHANG[3]*, Tianzu YANG[4], Dasha XIA[5]

This study explores the coordination behavior between azacrown ether and lanthanide rare earth ions in sulfate solution. Liquid-liquid solvent extraction experiments were carried out to determine the corresponding extraction parameter of the extraction distribution ratio D and the equilibrium constant K, both of them decreased gradually as the rare earth atomic number increased. Aza-crown ether, shows selective extraction ability for light rare earth ions in sulfate systems, can separate the low-concentration rare earth ions into light eare earth ions (LREs) and heavy rare earth ions (HREs) with the separation coefficient $\beta_{LREs/HREs}$ = 22.87. Density functional theory (DFT) calculations further demonstrate the steric hindrance and weak interactions between coordination atoms are the key factors influencing the structural stability of Ln(III)–2N15C5–H_2O, the ionic complexes of LREs and 2N15C5 has a more stable core–shell structure with shorter bond lengths and stronger interactions between coordination atoms.

Keywords: azacrown ether; lanthanide rare earth ions; density functional theory; coordination ability; liquid-liquid solvent extraction

1. Introduction

Molecular recognition technology based on supramolecular chemistry is a high-efficiency selective separation technology, which can design and synthesize ligand molecules for specific ion targets under the conditions of ion radius, coordination characteristics, spatial structure, etc. [1-2]. Among them, macrocycle crown ethers are the earliest and most thoroughly studied compounds for cationic recognition, and widely used in pharmaceutical synthesis [3], chemical catalysis [4], mineral recognition [5], element separation [6] and other fields.

In terms of the recognition and separation of metal ions by crown ethers, the recognition mechanism is mostly explained as the "best-fit" mechanism based on the cavity size matching effect [7], that is, the cavity formed by [-CH_2-CH_2-O-] in crown ether can be selectively combined with metal cations of right radii through

[1] School of metallurgy and environment, Central South University, Changsha 410008, Hunan, China. E-mail: wujianghua101@163.com, Senior engineer
[2] Changsha Research Institute of Mining and Metallurgy Co., Ltd., Changsha 410008, Hunan, China. E-mail: wujianghua101@163.com, Senior engineer
[3] School of metallurgy and environment, Central South University, Changsha 410008, Hunan, China. E-mail: zdc015@csu.edu.cn, Associate Professor, Master Supervisor
[4] School of metallurgy and environment, Central South University, Changsha 410008, Hunan, China. E-mail: tianzuyang@163.com, Professor, Doctoral supervisor
[5] Hangzhou Yanqu Information Technology Co., Ltd., Hangzhou 310012, Zhejiang, China. E-mail: xiadasha@hotmail.com, Senior engineer

ion-dipole interaction. The more the size matches, the stronger the bonding ability is. In addition to alkali metals [8-9], heavy metals [10], and platinum group metal ions [11-12], crown ethers also show good separation and recognition capabilities for lanthanide rare earth ions [13-16] in organic system. However, most reports on the complexation of Ln^{3+} by crown ethers and their derivatives are limited to chloride or nitrate dissolved into organic systems. There are few reports on the interaction between rare earth ions and crown ethers in sulfate aqueous system.

Lanthanide contraction causes the difference in radius size and electron density distribution between adjacent rare earth ions. Based on these differences, it is possible to achieve the grouped separation of Ln^{3+} through coordination recognition, such as lanmodulin protein [17] and metal-organic framework/ nanoporous graphene [18]. To date, the coordination mechanism between Ln^{3+} and crown ether derivatives are more attributed to element doping or chemical grafting, nearly no systematic research on the coordination rules between Ln^{3+} and ether rings.

In this paper, azacrown ether 2N15C5(1,7-Diaza-15 crown 5 ether) was selected as the main recognition macromolecular, and its coordination ability with 13 lanthanide rare earth ions in sulfate system was studied both by quantum chemistry simulation calculation and liquid-liquid extraction experiment, which aims to provide a new strategy for the separation of adjacent lanthanide rare earth ions in sulfate system.

2. Calculation and experiment

To simplify the calculation, a core-shell structure as shown in Fig.1 was constructed to simulate the coordination process of lanthanide rare earth ions and azacrown ether in aqueous solution. The inner core in fig.1(b) is a complexion of Ln(Ⅲ)-2N15C5-H_2O formed by the coordination of Ln(III)-H_2O and 2N-15C, and the outer shell is dominated by the electrostatic interaction between complexions and SO_4^{2-} to form a neutral complexes of Ln(Ⅲ)-2N15C5-H_2O-SO_4 in fig.1(c). The structure stability of the inner core is the key factor determining the stable existence of the neutral complex in solution.

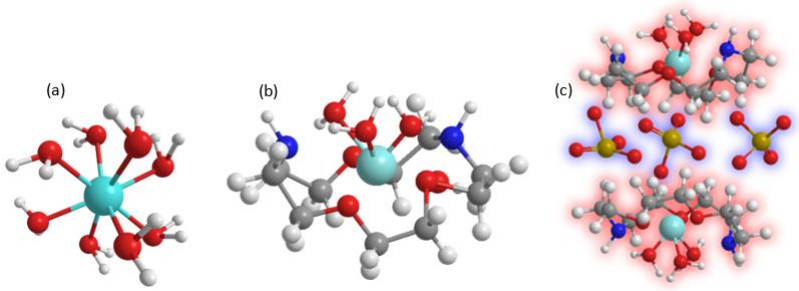

Fig. 1. Schematic diagram of coordination process of Ln^{3+} with 2N15C5 in sulfate system

2.1 Calculation method

The coordination interaction of $Ln(H_2O)_8^{3+}$ and 2N15C5 in simulated solution was calculated by Gaussion16[19]. According to the statistical data of coordination number of Ln^{3+} with nitrogen-containing and oxygen-containing ligands in the Cambridge structure database CSD[20] and the inorganic crystal structure database ICSD[21], the coordination number of Ln^{3+} with 2N15C5 in this paper is preferentially 8.

The geometric structures of Ln(III)-H_2O, 2N15C5 and Ln(Ⅲ)-2N15C5-H_2O were optimized at the B3LYP level with the pseudopotential group def2-SVP for Ln^{3+} and 6-311G(d) for 2N15C5[22]. The electron density topological analysis, molecular surface electrostatic potential (ESP) and independent gradient model analysis(IGMH) were analyzed by Multiwfn 3.8[23].

2.2 Exprement method

Liquid-liquid solvent extraction(LLE) was carried out to verify the reliability of calculation conclusions, and the experiment-conditions are as follows: 2N15C5 with a concentration of 0.0015mol/L in carbon tetrachloride solvent was used as the extractant, the aqueous phase was rare earth sulfate solution with 0.001 mol/L of various Ln^{3+}, pH=2. Extraction parameters for LLE are setted as: phase ratio O/A=1:1, room temperature 25°C, mixed-time of 30min and standing time of 1h, then the concentration of target ions in residual solution can be detected by ICP-MS (ICAP7400radial, Thermo Fisher Scientific Inc.). Three groups of parallel independent control tests were set up for each Ln^{3+}, and the average value of the test was taken as the final result.

3. Result and discussion

3.1 Reactivity of azacrown ether and Ln(III)-H_2O

The multidentate ligand 1,7-diaza-15-crown-5 ether(2N15C5) can be obtained by introducing nitrogen heteroatoms into the ring of conventional 15-crown-5 ether (15C5), as shown in Fig.2 (a, b). The formation of carbon-nitrogen triple bond causes the structure rearrangement and induces the diameter of ring cavity shrinking to 1.05-2.65Å (slightly less than 1.22-2.86Å of 15C5). It's very suitable to match with Ln^{3+} because the diameter ratio of Ln3+ and 2N15C5 is in the range of 0.9~1.4(Fig.2(d)) [24]. In particular, N and O atoms on the crown ether ring, as the extreme points of surface electrostatic potential, are the active sites of nucleophilic reaction. An obvious negative potential cavity in Fig.2(c) is formed in the center, which is easy to capture positively charged ions.

The ionic potential of Ln^{3+} in Ln(III)-H_2O is defined as the ratio of atom charge of Ln^{3+} to the effective radius of hydrated ions, as shown in Fig.2(d). In general, the higher the ionic potential of Ln^{3+} is, the stronger its binding with ligands

is, and the more stable the complex is [9]. According to the reactivity trend, there is a coordination binding ability between Ln(III)-H_2O and 2N15C5 due to 'best-fit' size matching effect and nucleophilic-electrophilic reaction.

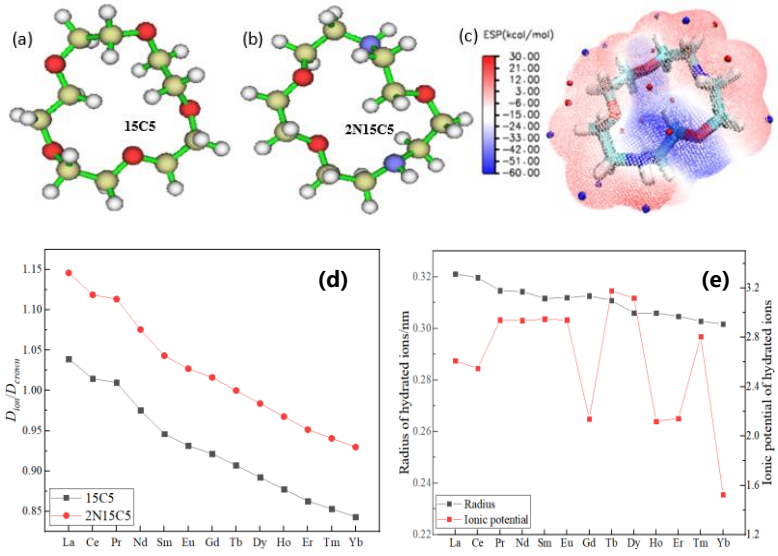

Fig. 2 (a&b) Structure of 15C5 and 2N15C5 (O and N atoms are shown in red and blue, respectively). c) Surface electrostatic potential of 2N15C5 (the red and blue colors indicate high and low electrostatic potential, respectively). (d)Diameter ratio of Ln^{3+} to crown ethers. (e) Radius and the ionic potential of Ln(III)–H_2O .

3.2 complexion structure and steric hindrance

The calculation results show that the configuration of Ln:2N15C5:H_2O=1：1：3 in complexions is the most stable, as shown in the insert figure of Fig. 3(a). In the complexions of Ln(III)-2N15C5-H_2O, Ln^{3+} is embedded right above the central of crown ether cavity and bonds with O and N atoms, and three water molecules lie on the other side of Ln^{3+} and bond with Ln^{3+} through O atoms, which forms a 'sandwich-like' semi-encapsulated structure.

The coordination of Ln(III)-H_2O with 2N15C5 in solution can be regarded as a competitive coordination process between Ln^{3+}-2N15C5 and Ln^{3+}-H_2O, including the following steps such as the cleavage of Ln-water oxygen bond(Ln-H_2O) and the formation of Ln-ether oxygen bond(Ln-O(L)) and Ln-ether nitrogen bond(Ln-N(L)). The geometry of Ln(III)-2N15C5-H_2O complexions is a balance between minimizing steric hindrance and maximizing coordination binding [25-26].

In Ln–2N15C5–H_2O, the average bond length decreased gradually as the rare earth atomic number increased: Ln–O(L) > Ln–O(H_2O) > Ln–N(L) [Fig. 3(a)]. When accounting for the Ln^{3+} ionic size, the modified inter-atomic distances of Ln–

N(L)–r(Ln), Ln–O(L)–r(Ln), and Ln–O(H_2O)–r(Ln) all increased as the rare earth atomic number increased [Fig. 3(b)].

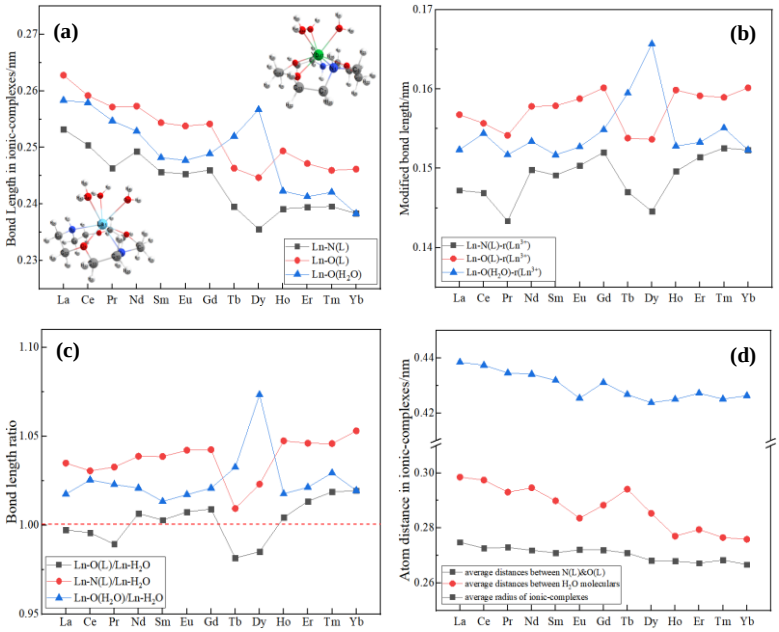

Fig.3 (a)Bond length and (b)Modified bond length of ionic-complexes; (c)Ratio of bond length ratio of ionic-complexes and hydrated ions; (d)Average atoms distances in ionic-complexes

Assuming a core-shell structure showed in Fig. 1 and the competitive coordination existing, when l(Ln–N(L))/l(Ln–H_2O) < 1 and/or l(Ln–O(L))/l(Ln–H_2O) < 1, the spatial structure between Ln^{3+} and 2N15C5 is more compact than that between Ln^{3+} and H_2O, such as the complexes involving La, Ce, Pr, Sm, Tb, and Dy which is located on and below the red dashed line in Fig. 3(c) . Meanwhile, due to the spatial repulsion between aza-crown ether and water molecules, the inner distance between Ln–O(H_2O) is much greater than that of Ln–H_2O in hydrate ions. Particularly, due to lanthanide contraction, the radii of Tb^{3+} and Dy^{3+} are much more compatible with the cavity size of 2N15C5 compared with the other cations [Fig. 2(d)， $D_{Tb/2N15C5}$=1.00, $D_{Dy/2N15C5}$=0.98], and the inner distance in Fig. 3(a) between Tb^{3+}/Dy^{3+} and N,O atoms of 2N15C5 is shorter than those for others.

The structural rearrangement of an ionic complex also changes the inter-atomic distance between the ligand N and O atoms. As shown in Fig. 3(d), the average radius of ionic-complexes, the average distances between N and O atoms in the crown ether ring as well as between water oxygen atoms, decrease gradually with varies degree as the rare earth atomic number increases. This indicates that 2N15C5 and water molecules gradually aggregate to two ends of ionic complexes. A looser structure corresponds to lower ionic complex stability. Moreover, the lengths of the Ln–N(L), Ln–O(L), and Ln–O(H_2O) bonds are over 1.15 times greater than the

theoretical covalent radius [27]. Thus, there are no strong chemical bonds between Ln^{3+} and N/O coordination atoms.

3.3 Electron density and weak interactions

The complexation between Ln^{3+} and 2N15C5 inevitably results in changes in electron density between coordination atoms. In the atoms in molecules (AIM) theory, the bond critical point (BCP) is an important indicator of the interaction strength between coordination atoms, and the electron density $\rho(r)$ at the BCP is positively correlated with the bonding strength [28-29].

The Laplacian operator $\nabla^2\rho(r)$ over the BCP between coordination atoms can reflect the interaction properties in ionic complexes [30]. As shown in Fig. 4(a), the $\nabla^2\rho(r)$ values of Ln–N(L), Ln–O(L), and Ln–O(H_2O) are concentrated in the range of 0.10–0.25, which is similar to the values observed for the standard metal–organic complexes with weak interactions ($\nabla^2\rho(r)$ = 0.15–0.25) [31].

The strength of a weak interaction between coordination atoms is positively correlated with the electron density at the BCP [32-33]. For charged ionic complexes, the electron density ρ(r) at the BCP exhibits a good linear correlation with the weak interaction ΔE (kcal/mol) [34]:

$$\Delta E = -332.34 \times \rho(BCP) - 1.0661. \quad (1)$$

As shown in Fig. 4(b), the weak interactions of Ln–O(L), Ln–N(L), and Ln–O(H_2O) are strong with $|\Delta E|$ > 15.0 kcal/mol, indicating both electrostatic attraction and disperse force, induced force between coordination atoms. The weak interaction between Ln–O(L), Ln–N(L) in the ionic-complexes is significantly stronger than that between Ln–H_2O in hydrated ions.

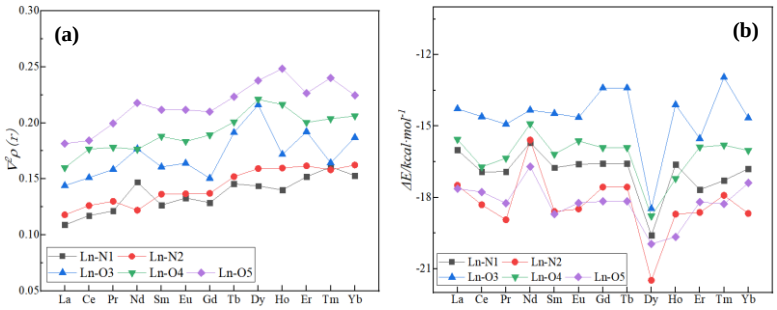

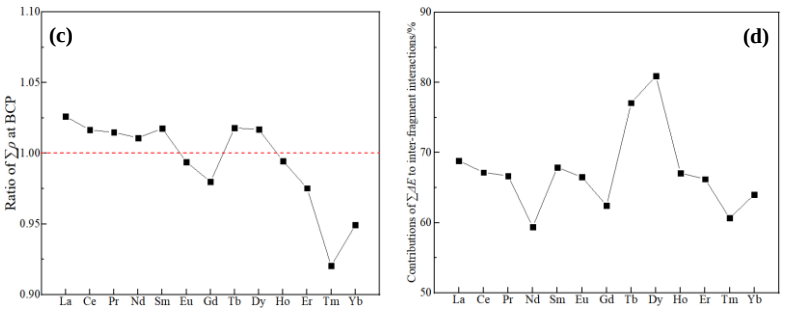

Fig. 4. The Topological analysis of ploy-ions(a):Laplacian operator at BCP; b): Weak interaction at BCP in ionic-complexes; c): Electron density ratio at BCP of complex-ions and hydrate-ions; d):Contribution of $\sum\Delta E$ to inter-fragment interactions)

The structural stability of ionic-complexes depends on the strength of weak interactions between coordinating atoms. Based on the competitive coordination between Ln^{3+}–2N15C5 and Ln^{3+}–H_2O, if the sum of weak interactions at BCP in ionic-complex is greater than that between the corresponding hydrated ions, the ionic-complex can be stably formed. As shown in Fig.4(c), only La, Ce, Pr, Nd, Sm, Tb and Dy which are located above the red dotted line, satisfy the relationship of $\sum(\rho(Ln–N(L))+\rho(Ln–O(L)+\rho(Ln–O(H_2O)))/\sum \rho(Ln–H_2O) \geq 1$. Furthermore, the strenght of weak interaction between coordination atoms at BCP in Fig.4(b) and the contribution of weak interaction to the inter-fragments between Ln^{3+} and 2N15C5 in Fig. 4(d), clearly indicate that the ionic-complex of LREs is much stable than that of HREs. Independent gradient model based on Hirshfeld partition (IGMH) [35] of each coordination atoms in complex-ions can visualize the weak interaction between Ln(III)-H_2O fragments and 2N15C5 fragments, as shown in Fig.5(a). There are mainly attraction force in blue between Ln^{3+} and crown ether ring, which is reified as the ion-dipole interaction between Ln^{3+} and N and O atoms. Between adjacent N and O atoms (red) in crown ether ring there exists a weak steric repulsion in red, and the green vander Waals force manifests between water molecules and crown ether rings.

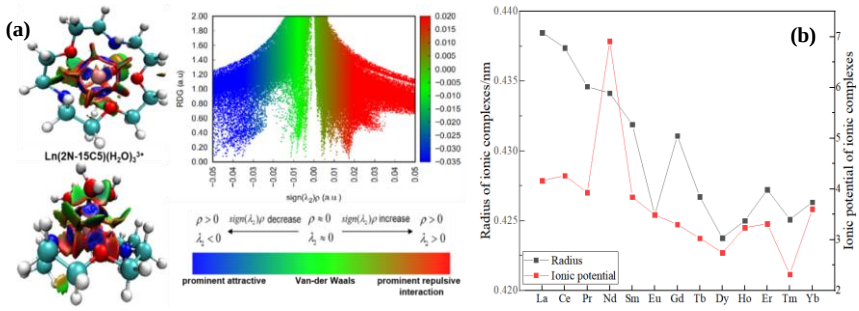

Fig.5. (a):The weak interactions between two fragments in complex-ions(RDG=0.6 [22-23]); (b)Average radius and ionic potential of ionic-complexes.

The ultimate goal of interaction between inter-fragments within complex is to iterate complementary intramolecular electrostatic and polarization effects to self-consistency [36] . The interaction between inter-fragments affects the electrostatic binding between charged ionic-complexes and equilibrium anions through the surface electrostatic potential (ESP) distribution, and finally determines the structural stability of rare earth-crown ether complexes. As shown in Fig.5(b), the average radius of ionic-complexes and their corresponding ionic potential both decrease gradually from La to Yb, leading to a decreasing trend in the electrostatic interaction between Ln(III)–2N15C5–H_2O and equilibrium anions.

In summary, the coordination of Ln^{3+} and 2N15C5 in solution is the comprehension effect of Lewis soft and hard acid-base interaction, electrostatic interaction between coordination atoms, dehydration of lanthanide rare earth ions, and ligand steric hindrance. 2N15C5 coordinates more strongly with LREs than HREs in a sulfate solution. This can be attributed to the shorter bond lengths between coordination atoms in the ionic complexes with LREs along with the stronger interactions at the BCP and more stable core–shell structure. However, due to the implicit solvent model adopted in the DFT calculation, the interactions between water molecules, aza-crown ether and equilibrium anions are not necessarily considered, the calculation conclusion of the structure stability of ionic-complexes only provide qualitative support but cannot achieve numerical agreement with the experimental results .

3.4 Determination of coordination constants

The extraction of Ln^{3+} by 2N15C5 includes three steps: dissolution of crown ether in aqueous phase, complexation reaction on the two-phase interface of aqueous and organic, the dissolution of complex in organic phase, and the reaction equation corresponding to each step is follows:

$$2N15C5_{(O)} \Leftrightarrow 2N15C5_{(aq)} \quad (5)$$

$$Ln(H_2O)_8^{3+} + x2N15C5_{(aq)} + ySO_4^{2-} = Ln(2N15C5)_x(H_2O)_n(SO_4)_y^{3-2y}{}_{(aq)} + (8-n)H_2O \quad (6)$$

$$Ln(2N15C5)_x(H_2O)_n(SO_4)_y^{3-2y}{}_{(aq)} \Leftrightarrow Ln(2N15C5)_x(H_2O)_n(SO_4)_y^{3-2y}{}_{(O)} \quad (7)$$

The extraction distribution ratio D of Ln^{3+} is calculated as follows:

$$D = \frac{[Ln(2N15C5)_x(H_2O)_n(SO_4)_y^{3-2y}]_{(O)}}{[Ln^{3+}]_{(aq)}} \quad (8)$$

Extraction distribution ratio *D* depends on the coordination binding ability between 2N15C5 and Ln^{3+}, and the corresponding experiment results of liquid-liquid solvent extraction are shown in Table 2.

Table 1

Distribution ratio of 2N-15C5 to Lanthanide rare earth ions in sulfate systems

Ln^{3+}	La^{3+}	Ce^{3+}	Pr^{3+}	Nd^{3+}	Sm^{3+}	Eu^{3+}	Gd^{3+}
Extraction distribution *D*	47.51	8.97	10.11	4.56	1.62	2.23	0.36
Ln^{3+}	Tb^{3+}	Dy^{3+}	Ho^{3+}	Er^{3+}	Tm^{3+}	Yb^{3+}	Lu^{3+}
Extraction distribution *D*	1.50	1.76	0.05	-0.01	-0.02	0.02	--

Note: -- means undetected.

The extraction ability of LREs by 2N15C5 in sulfate system is significantly higher than HREs. When the measured value of *D* below 1, the coordination reaction is weak, and it can be regarded that rare earth ions such as Gd^{3+}, Ho^{3+}, Er^{3+}, Tm^{3+}, Yb^{3+} cannot be extracted by 2N15C5 when considering the detection derivation of low-concentration Ln^{3+}.

The extraction equilibrium constant K is calculated as follows:

$$K = \frac{[Ln(2N15C5)_x(H_2O)_n(SO_4)_y^{3-2y}]_{(O)}}{[Ln^{3+}]_{(aq)}\cdot[2N15C5]^x_{(aq)}\cdot[SO_4^{2-}]^y_{(aq)}} \quad (9)$$

K is not only proportional to the extraction distribution ratio *D*, but also closely related to the solubility of ligand in organic and the concentration of equilibrium anions. Bringing Equa.(9) into Equa.(8) and taking logarithm on both sides to get Equa.(10) as below, the stoichiometric coefficient x and y can be obtained according to the slope of lg*D*-lg[*2N15C5*] and lg*D*-lg[SO_4^{2-}] curves.

$$\lg D = \lg K + y\lg[SO_4^{2-}] + x\lg[2N15C5] \quad (10)$$

When setting the concentration of sulfate ions is 2.5 times that of Ln^{3+} in the aqueous phase, the concentration of 2N15C5 is 1.5 times, 3 times, 6 times and 10 times of Ln^{3+}, thus the corresponding results of lg*D*-lg[*2N15C5*] curves are shown in Table 2. Since the actual concentration of 2N15C5 cannot be effectively determined, the residual concentration of 2N15C5 is approximately regarded as the difference between the original concentration in organic phase and the concentration consumed by coordination reaction. The slope of the fitting curve of lgD-lg[2N15C5] fluctuated in the range of 0.88-1.22, therefore x=1 was approximated considering the influence of ion concentration analysis deviation.

Table2

lg*D*-lg[*2N15C5*] curve of $Ln(H_2O)_8^{3+}$ extracted by 2N15C5

Ln^{3+}	**Fitting equation of lg*D*-lg[*2N15C5*] curve**	**R^2**	**x**
La^{3+}	y=1.0102x+2.9765	0.9934	1.0102
Pr^{3+}	y=0.8867x+2.1303	0.9946	0.8867

Nd^{3+}	y=1.2263x+2.1876	0.9751	1.2263
Eu^{3+}	y=1.1813x+1.8659	0.9851	1.1813

Furthermore, the concentration of SO_4^{2-} was adjusted to 2.5 times, 5 times, 7.5 times and 10 times the molar concentration of rare earth ions by adding high-grade pure sodium sulfate powder in aqueous phase. The results of the lg*D*-lg[SO_4^{2-}] fitting curve are shown in Table 3, thus the stoichiometric parameter can be regarded as y=1.5.

Table3

lgD-lg[SO_4^{2-}] curve of $Ln(H_2O)_8^{3+}$ extracted by 2N15C5

Ln^{3+}	Fitting equation of lgD-lg[SO_4^{2-}] curve	R^2	y
La^{3+}	y=1.5679x+4.2904	0.9974	1.5679
Ce^{3+}	y=1.4999x+3.7572	0.9998	1.4999
Pr^{3+}	y=1.4908x+3.9576	0.9999	1.4908
Nd^{3+}	y=1.5345x+3.5083	0.9999	1.5345
Sm^{3+}	y=1.5453x+3.1587	0.9996	1.5453
Eu^{3+}	y=1.5202x+3.2640	0.9991	1.5202

Above all, the extraction reaction formula of LREs by 2N15C in sulfate system is as follows:

$$Ln(H_2O)_8^{3+} + 2N15C5_{(O)} + 1.5SO_4^{2-} \Leftrightarrow Ln(2N15C5)(H_2O)_3(SO_4)_{1.5(O)} + 5H_2O \quad (11)$$

where *Ln*=La, Ce, Pr, Nd, Sm, Eu. Obviously, sulfate ion participates into the composition of complex, which can also be further confirmed by the Fourier Transform-Infrared spectrum in Fig.6.

Compared with 2N15C5, the N-H peak in 3330cm^{-1}, 1640cm^{-1} and 940cm^{-1} of extracted complex (La(III)-2N15C5-H_2O-SO_4) was significantly weakened, the C-N peak is blue-shifted and superimposed with the O-C-O characteristic peak in 1120cm^{-1},thus its strength and width are significantly increased, and making the characteristic peak of -CH_2 group migrated from 2890cm^{-1} to 2920cm^{-1}. A wide and strong H_2O characteristic peak appears at 3450cm^{-1} and a distinct hydrogen bond peak occurs at 1660cm^{-1}. These changes mostly indicate that C and N atoms of 2N15C5 and water molecules are all involved in coordination. Furthermore, the peak in 1390cm^{-1} and 590cm^{-1} are the asymmetric telescopic vibration and symmetrical telescopic vibration absorption band of sulfonic acid group, which indicates that sulfate ions were involved in the composition of extracted complex.

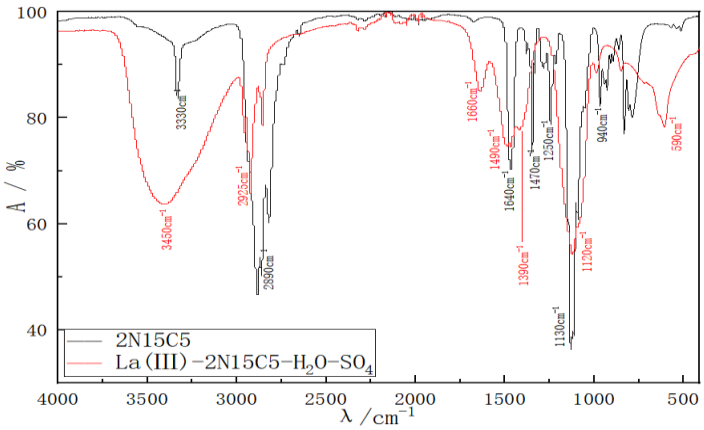

Fig.6. FTIR characterization results of 2N15C5 and La (III)-2N15C5-H_2O

When substituting the concentration values of Ln^{3+} of aqueous phase before and after extraction into Equa.(11), the corresponding logarithmic value of extraction equilibrium constant can be calculated as shown in Table 4. It's indicative that the coordination binding between LREs and 2N15C5 is stronger than that in the ionic complexes of HREs.

Table 4

Extraction equilibrium constant logarithm (lg*K*) of Ln (III)-2N15C5-H_2O-SO_4

Ln^{3+}	Measured data	Reference data[a]	Reference data[b]	Ln^{3+}	Measured data	Reference data[a]
La^{3+}	5.65	6.49	5.17	Tb^{3+}	3.92	5.96
Ce^{3+}	5.33	--	4.62	Dy^{3+}	3.85	--
Pr^{3+}	5.46	6.22	4.45	Ho^{3+}	3.09	5.66
Nd^{3+}	5.02	6.55	3.93	Er^{3+}	2.61	5.33
Sm^{3+}	4.26	6.11	2.81	Tm^{3+}	2.06	--
Eu^{3+}	4.74	--	2.26	Yb^{3+}	1.37	5.53
Gd^{3+}	3.50	--	2.03			

Note: Literature data[a] and Literature data[b] are the logarithm of complex stability constant for complexation of $Ln(CF_3SO_3)_3$ with 2N15C5 in propylene carbonate system [37] and complexation of $Ln(NO_3)_3$ with 15C5 in anhydrous acetonitrile system [38] in 25°C.

As shown in Table 4, the trend of experimental measured data is consistent with the literature data. The quantitative difference is mainly attributed to the types of rare earth salts and reaction systems, since the solubility or dissociation of lanthanide rare earth salts in solvents will directly affect the coordination of Ln^{3+} with crown ether ligands [37]. 2N15C5 shows much weaker complexation ability for $Ln_2(SO_4)_3$ than that of $Ln(CF_3SO_3)_3$ in Ref.37, mainly due to the strong solvation effects caused by the different solubility of rare earth salts in aqueous and propylene carbonate respectively; the big solvation effect between ligand and solvent

molecular can significantly influence the weak interaction between coordination atoms. Compared with the corresponding value in Ref.38, 2N15C5 shows a little greater complexation ability for Ln^{3+} is attributed to the balance of following two effects, 2N15C5 has a stronger nucleophile reaction ability than 15C5[Fig. 2(d)], however there is a competing coordination to Ln^{3+} between solvent molecules and 2N15C5.

4. Conclusions

The introduction of nitrogen heteroatoms on crown ether ring can cause structure to rearrange, thus significantly enhancing its nucleophilic reactivity. Azacrown ether shows great selective coordination ability for light rare earth ions in sulfate systems.

Base on DFT calculation, azacrown ether can coordinate with Ln^{3+} to form a "sandwich-like" semi-encapsulated complexions of Ln:2N15C5:H_2O=1:1:3. The steric hindrance caused by size matching and the weak interaction between coordination atoms are the key factors which influence the structural stability of Ln(III)-2N15C5- H_2O complexions with core-shell structure. When coordination with light rare earth ions, the bond length between 2N15C5 and Ln^{3+} is shorter, the electron density is larger, the weak interaction is much stronger, and the corresponding complexions Ln(III)-2N15C5-H_2O of La^{3+}, Ce^{3+}, Pr^{3+}, Tb^{3+}, Dy^{3+} are more stable. The extraction parameters of lanthanide rare earth ions by azacrown ether in sulfate solution determined by liquid-liquid solvent extraction is basically consistent with the calculation conclusion. 2N15C5 has good extraction ability to light rare earth ions in sulfate solution, and sulfate ions participates into the composition of extracted complexes.

Acknowledgment

This work was financially supported by the National Natural Science Foundation of China (51704039) and Natural Science Foundation of Hunan Province (2017JJ3320).

R E F E R E N C E

[1] K. Ariga, H. Ito, J. P. Hill, H. Tsukube.Molecular recognition: from solution science to nano/ materials Technology, Chemical Society Reviews. 41(2012): 5800-5835.

[2] J. S. Bradshaw, R. M. Izatt, P. B. Savage, R. L. Bruening, K. E. Krakowiak. The Design of Ion Selective Macrocycles and the SolidPhase Extraction of Ions Using Molecular Recognition Technology: A Synopsis, Supramolecular Chemistry. 12(2000): 23-26.

[3] S. Dong, Y. Luo, X. Yan, B. Zheng, X. Ding, Y. Yu, Z. Ma, Q. Zhao, F. Huang. A dual-responsive supramolecular polymer gel formed by crown ether based molecular recognition, Angewandte Chemie International Edition. 50(2011): 1905-1909.

[4] A. C. Deacy, E. Moreby, A. Phanopoulos, C. K. Williams. Co(III)/ Alkali-Metal(I) Heterodinuclear Catalysts for the RingOpening Copolymerization of CO2 and Propylene Oxide, Journal of the American Chemical Society. 2020.

[5] J. E. Sutton, S. Roy, A. U. Chowdhury, L. Wu, A. K. Wanhala, N. D. Silva, S. J. Popova, B. P. Hay, M. C. Cheshire, T. L. Windus, A. G. Stack, A. Navrotsky, B. A. Moyer, B. Doughty, V. S. Bryantsev. Molecular Recognition at Mineral Interfaces: Implications for the Beneficiation of Rare Earth Ores, ACS Applied Material Interfaces. 12(2020):16327-16341.
[6] R.M. Izatt, J.S. Bradshaw, R.L. Bruening, B. J. Tarbet, and M.L. Bruening. Solid phase extraction of ions using molecular recognition technology, Pure and Applied Chemistry. 67(1995): 1069-1074.
[7] M R Izatt, P D Nelson, H J Rytting. Calorimetric study of the interaction in aqueous solution of several uin-and bivalent metal ions with the cyclic polyether dicyclohexyl-18-crown-6 at 10, 25 and 40, Journal of the Americal Society. 93(1971): 1619-1623.
[8] Y. Tian, W. Chen, Z. Zhao, L. Xu, B. Tong. Interaction and selectivity of 14-crown-4 derivatives with Li+ , Na+, and Mg2+ metal ions, Journal of Molecular Modeling. 26(2020): 67.
[9] Z. Jing, G. Wang, Y. Zhou, D. Pang, F. Zhu , H. Liu. Selectivity of 18-crown-6 ether to alkali ions by density functional theory and molecular dynamics simulation, Journal of Molecular Liquids. 311(2020): 113305.
[10] S R Izatt, N E Izatt, R L Bruening. Metal separations of interest to Chinese metallurgical industry, Journal of Rare Earths. 28(2010): 22-29.
[11] R M Izatt, S R Izatt, N E Izatt, et al. Industrial applications of molecular recognition technology to separations of platinum group metals and selective removal of metal impurities from process streams, Green Chemistry. 17(2015): 2236-2245.
[12] R. E. C. Torrejos , E. C. Escobar, J. W. Han, S. H. Min, H. Yook, K. J. Parohinog, S. Koo, H. Kim, G. M. Nisola, W. Chung. Multidentate thia-crown ethers as hyper-crosslinked macroporous adsorbent resins for the efficient Pd/Pt recovery and separation from highly acidic spent automotive catalyst leachate, Chemical Engineering Journal. 424(2021): 130379.
[13] S. R. Dave, H. Kaur, S. K. Menon. Selective solid-phase extraction of rare earth elements by the chemically modifified Amberlite XAD-4 resin with azacrown ether, Reactive & Functional Polymers. 70(2010): 692-698.
[14] H. Okamura, N. Hirayama, K Morita, K. Shimojo, H. Naganawa, H Imura. Synergistic Effect of 18-Crown-6 Derivatives on Chelate Extraction of Lanthanoids(III) into an Ionic Liquid with 2-Thenoyltrifluoroacetone, Analytical Sciences. 26(2010): 607-611.
[15] B. V. Zhmud, A. A. Golub, V. G. Pivovarenko. Synthesis and Study of Ion Adsorption and Fluorescent Properties of Silica-Grafted Bis(crown azo)methine[J]. Inorganic Materials. 40(2004): 1006-1013.
[16] V. V. Yakshin, V. I. Zhilov, S. V Demin, G. A. Pribylova, I. G. Tananaev, A. Y. Tsivadze, B. F. Myasoedov. Extraction of Am and rare-earth elements from acidic solutions by alkyl derivatives of dibenzo- and dicyclohexano-18-crown-6, Comptes Rendus Chimie. 10(2007): 1020-1025.
[17] Dong, Z.Y., Mattocks, J.A., Deblonde, G.J.-P., Hu, D.H., Jiao, Y.Q., Cotruvo Jr., J.A., Park, D.M., 2021. Bridging Hydrometallurgy and Biochemistry: A Protein-Based Process for Recovery and Separation of Rare Earth Elements, ACS Cent. Sci., 7, 11, 1798–1808. https://doi.org/10.1021/acscentsci.1c00724
[18] Wu, J.S., Li, Z., Tan, H.X., Du, S.B., Liu, T.Q., Yuan, Y.L., Liu, X.H., Qiu, H.D., 2021. Highly selective separation of rare earth elements by Zn-BTC metal−organic framework/ nanoporous graphene via in situ green synthesis, Anal. Chem. 93, 3, 1732–1739. https://doi.org/10.1021/acs.analchem.0c04407
[19] M. J. Frisch, G. W. Trucks, H. B. Schlegel, et. al. Gaussian 16, Lnvision C.01, Gaussian, Inc., Wallingford CT, 2019.
[20] Allen F H (2002) Acta Crystallogr., Sect. B 58:380-388; CSD ConQuest build 1.19
[21] Hellenbrandt M(2014) The inorganic crystal structure database (ICSD)—present and future; ICSD 1.4.6 (release: 2017-1)
[22] T. Lu. Multiwfn SoftwaLn Manual(Version 3.8), 2020-Feb-8.
[23] T. Lu, F. Chen. Multiwfn: a multifunctional wavefunction analyzer, Journal of Computational Chemistry, 2012, 33: 580-592.

[24] Mao, J.G., Jin, Z.S., Ni, J.Z.. Cavity of the crown ether and its relationship with the structure of rare earth nitrate complexes, Eur. J. Inorg. Chem., 1994, 10, 4, 339-345.
[25] E. N. Rizkalla, G. R. Choppin. Chapter 103 Hydration and hydrolysis of lanthanides, Handbook on the Physics and Chemistry of Rare Earths Volume 15(edited by K A Gschneidner, Jr L Eyring), 1991: 393-442.
[26] P. Starynowicz. Two complexes of Sm(II) with crown ethers— electrochemical synthesis, structure and spectroscopy, Dalton Transation. 5(2004): 825-832.
[27] T. Lu, F. Chen. Bond Order Analysis Based on Laplacian of Electron Density in Fuzzy Overlap Space, Journal of Physical Chemistry A. 117(2013): 3100-3112.
[28] E. R. Johnson, S. Keinan, P. Mori-Sánchez, J. Contreras-García, A. J. Cohen, W. Yang. Revealing noncovalent interactions, Journal of the American Chemical Society. 132(2010): 6498-6506.
[29] R. F. W. Bader. Atoms in Molecules, A Quantum Theory, International Series of Monographs in Chemistry, vol. 22, Oxford University Press, Oxford, 1990.
[30] T. Lu, F. Chen. Bond Order Analysis Based on Laplacian of Electron Density in Fuzzy Overlap Space, Journal Physical Chemistry A. 117(2013): 3100-3108.
[31] U. Koch, P. L. A. Popelier. Characterization of C-H-O Hydrogen Bonds on the Basis of the Charge Density, The Journal of Physical Chemistry. 99(1995): 9747-9754.
[32] C. Lefebvre, G. Rubez, H. Khartabil, J. C. Boisson, J. ContrerasGarcía, E. Hénon. Accurately extracting the signature of intermolecular interactions present in the NCI plot of the reduced density gradient versus electron density, Physical Chemistry Chemical Physics. 19(2017): 17928-17936.
[33] F. Zhou, Y. Liu, Z. Wang, T. Lu, Q. Yang, Y. Liu, B. Zheng. A new type of halogen bond involving multivalent astatine: an abinitio study, Physical Chemistry Chemical Physics. 21(2019): 15310-15318.
[34] S. Emamian, T. Lu, H. Kruse, H. Emamian. Exploring Nature and Predicting Strength of Hydrogen Bonds: A Correlation Analysis Between Atoms-in-Molecules Descriptors, Binding Energies, and Energy Components of Symmetry-Adapted Perturbation Theory, Journal of Computational Chemistry. 40(2019), 2868-2881.
[35] Lu, T., Chen, Q.X., 2022. Independent gradient model based on Hirshfeld partition: A new method for visual study of interactions in chemical systems, J. Comput. Chem., 43, 8, 539-555. https://doi.org/10.1002/jcc.26812
[36] Murray, J.S., Politzer, P., 2017. Molecular electrostatic potentials and noncovalent interactions, Wires Comput. Mol. Sci., e1326. https://doi.org/10.1002/wcms.1326
[37] P. D. Bernardo, A. Melchior, M. Tolazzi, P. L. Zanonato. Thermodynamics of lanthanide(III) complexation in non-aqueous solvents, Coordination Chemistry Reviews. 256(2012): 328-351.
[38] Liu, Y., Han, B. H., Chen, Y. T., 2000. The complexation thermodynamics of light lanthanides by crown ethers. Coordin. Chem. Rev., 200-202, 53-73. https://doi.org/10.1016/S0010-8545(99)00239-8